

N_2^+ Lasing: Gain and Absorption in the Presence of Rotational Coherence

Marianna Lytova,^{1,2,*} Maria Richter,³ Felipe Morales,³ Olga Smirnova,^{3,4} Misha Ivanov,^{3,5,6} and Michael Spanner^{1,2,†}

¹*National Research Council of Canada,*

100 Sussex Drive, Ottawa ON K1A 0R6, Canada

²*Department of Physics, University of Ottawa, Ottawa, Canada, K1N 6N5*

³*Max-Born Institute, Max-Born-Strasse 2A, D-12489, Berlin, Germany*

⁴*Technische Universität Berlin, Ernst-Ruska-Gebäude,*

Hardenbergstraße 36A, 10623 Berlin, Germany

⁵*Blackett Laboratory, Imperial College London,*

SW7 2AZ London, United Kingdom

⁶*Department of Physics, Humboldt University,*

Newtonstraße 15, D-12489, Berlin, Germany

(Dated: April 9, 2020)

Abstract

We simulate the pump-probe experiments of lasing in molecular nitrogen ions with particular interest on the effects of rotational wave-packet dynamics. Our computations demonstrate that the coherent preparation of rotational wave packets in N_2^+ by an intense short non-resonant pulse results in a modulation of the subsequent emission from $B^2\Sigma_u^+ \rightarrow X^2\Sigma_g^+$ transitions induced by a resonant seed pulse. We model the dynamics of such pumping and emission using density matrix theory to describe the N_2^+ dynamics and the Maxwell wave equation to model the seed pulse propagation. We show that the gain and absorption of a delayed seed pulse is dependent on the pump-seed delay, that is, the rotational coherences excited by the pump pulse can modulate the gain and absorption of the delayed seed pulse. Further, we demonstrate that the coherent rotational dynamics of the nitrogen ions can cause lasing without electronic inversion.

* mlytova2@uottawa.ca

† michael.spanner@nrc.ca

I. INTRODUCTION

Laser-induced molecular alignment of polarizable molecules was first considered by Friedrich and Herschbach [1]. This initial work was followed by numerous experimental and theoretical studies that further developed the scope of laser-induced molecular alignment [2–4]. An important result was the realization that ultrashort pulses could be used to generate time-dependent alignment that persists after the initial laser pulse has past [5–7], a phenomenon called rotational wave-packet revivals [8, 9]. The rotational revivals can in turn be used to shape and control light pulses propagating through the rotationally excited medium, e.g., for pulse compression down to the single-cycle limit [10, 11] through spectral broadening and shaping, or creating quantum optical memory [12] by forcing absorption and emission of light. In this paper, we explore the effects of rotational wave packets on the absorption and amplification of a delayed seed pulse propagating through a rotationally-excited gas of N_2/N_2^+ molecules. Such a system arises naturally in the so-called air laser, a phenomenon that was originally observed in 2003 in laser filaments driven by ultrashort strong laser pulses propagating in air [13], and has recently become subject of numerous advanced experimental studies [14–25].

Following the initial observations, the lasing process was generalized to a pump-probe scheme where a strong pump pulse ionizes and excites N_2 gas followed by a seed pulse that is amplified at selected wavelengths [14, 15]. More specifically, the seeded process proceeds as follows First, the leading edge of the pump pulse exerts a torque on the neutral nitrogen molecules towards the laser polarization direction, preparing coherent rotational wave packets in N_2 . Near the peak of the pump, a fraction of the rotationally excited molecules is strong-field ionized, producing rotationally excited N_2^+ ions in the ground ($X^2\Sigma_g^+$) and lowest excited ($A^2\Pi_u$, $B^2\Sigma_u^+$) electronic levels that are driven further during the trailing edge of the pulse. The weak seed pulse that follows is tuned to the $B^2\Sigma_u^+ \leftrightarrow X^2\Sigma_g^+$ transition energy in N_2^+ (391 nm). It is seen to undergo exponential gain [14], which, with varying seed delay, is modulated by the long-lived rotational dynamics of the ions induced during the pump step [17]. The observed gain of the time-delayed seed is widely held as evidence that the pump pulse creates population inversion between the $B^2\Sigma_u^+$ and $X^2\Sigma_g^+$ states in the ion [16], but also inversionless mechanisms [26] have been proposed to cause the amplification.

In this paper, we explore the process of absorption and gain of the seed pulse in the

presence of coherent rotational excitations, which is the transient inversion induced by the rotational wave packets evolving on the $X^2\Sigma_g^+$ and $B^2\Sigma_u^+$ surfaces proposed in Ref.[25]. This process is effectively a manifestation of ultrafast lasing without inversion scenarios [27–29]. There are two key ingredients that make N_2^+ lasing possible without inversion. First, the parallel coupling between the $X^2\Sigma_g^+$ and $B^2\Sigma_u^+$ states; molecules that are aligned with the seed polarization absorb and emit more efficiently than those perpendicular to it. Second, the different rotational constants of the ionic states that lead to a temporal offset in their rotational evolutions. There will be moments in time where the molecules in the $B^2\Sigma_u^+$ state are preferentially aligned with the seed polarization while those in the $X^2\Sigma_g^+$ are preferentially aligned perpendicular, thus giving an advantage to the emission from $B^2\Sigma_u^+$ over the absorption from $X^2\Sigma_g^+$ even in the absence of electronic inversion. Thus, the lasing regime can be achieved due to rotational wave packet evolution of the excited and ground states, even if there is no explicit electronic population inversion. Based on this idea, the authors of Ref.[25] proposed the condition of lasing in the form $p_B \langle \cos^2 \theta \rangle_B(t) > p_X \langle \cos^2 \theta \rangle_X(t)$, i.e. the product of the population and the molecular alignment measure for the excited state $B^2\Sigma_u^+$ is higher than the same parameter in the ground state $X^2\Sigma_g^+$. Here, we develop computational models that confirm the role of the rotational transient inversion mechanism [25].

II. COMPUTATIONAL MODEL

Our interest is to investigate the gain/absorption process of a delayed seed in the presence of the rotationally-excited $X^2\Sigma_g^+$ and $B^2\Sigma_u^+$ ionic states. To this end, we start by modeling the generation of the rotational wave packets by the pump pulse. Both the initial rotational excitation in the neutral and subsequent rotational excitation in the ion states following ionization are computed. Focusing primarily on the effects of the rotational coherences on the gain process, we do not attempt to fully model the possible inversion generated by the pump pulse in the present study, but take the liberty to vary the relative populations of the ionic states directly to seeing how the rotational coherences can affect the gain/absorption process in both inverted and non-inverted scenarios. With this goal in mind, we also omit the inclusion of the $A^2\Pi_u$ electronic state in N_2^+ which is known to cause depletion of the $X^2\Sigma_g^+$ state population through a one-photon coupling [19, 20], since we are instead choosing

to set the $X^2\Sigma_g^+$ and $B^2\Sigma_u^+$ populations by hands. Our treatment of rotational lasing without inversion in N_2^+ that includes a more complete modeling of the pump pulse excitation is presented elsewhere [30]. After the pump pulse has generated the rotationally-excited medium, we then solve the coupled Maxwell/von Neumann equations for the propagation of the seed pulse through the excited medium in order to calculate the gain and/or absorption of the seed.

We choose to model the quantum system using a density matrix approach. First, in the case where there is an initial thermal distribution, we have found the density matrix approach to be computationally faster than using the Schrödinger equation; the latter requires averaging over separate simulations for each rotational state in the initial ensemble, while the former can group many incoherently populated initial rotational states into a single simulation. Second, using a density matrix approach allows us to naturally incorporate the case where the $X^2\Sigma_g^+$ and $B^2\Sigma_u^+$ states of the ion have no initial coherence relative to each other, which is necessary to model the physical situation where the system does not emit unless the emission is triggered by a seed. The following outlines the details of our model for this study.

A. Level Structure and Initial Conditions

In the remainder of the paper, we refer to the neutral state $X^1\Sigma_g^+$ and the ionic states $X^2\Sigma_g^+$ and $B^2\Sigma_u^+$ as N , X and B . Their energy levels are written in standard form [31]:

$$\begin{aligned} \mathcal{E}_J = & T_e + (B_e - \frac{\beta_e}{2})J(J+1) - D_eJ^2(J+1)^2 \\ & + \omega_e(\nu + \frac{1}{2}) - X_e\omega_e(\nu + \frac{1}{2})^2 + Y_e\omega_e(\nu + \frac{1}{2})^3, \end{aligned} \quad (1)$$

where the rotational and vibrational constants are summarized in Table I. We designate the ro-vibronic energies of N , X and B as E_J^N , E_J^X and E_J^B , respectively. The minimum electronic energies, T_e , of N and X are set to zero, while for B we use $T_e=25461.4 \text{ cm}^{-1}$. For the neutral, we neglect the vibrational corrections to the rotational energies. The energies of the P- and R-branches are presented in Fig. 1, with the inset illustrating the definition of both branches. We include only the ground vibrational state ($\nu = 0$) of each electronic state in the current model, which corresponds to the 391 nm transition in N_2^+ .

The initial N_2 medium is taken to be at room temperature ($T = 298 \text{ K}$) with number

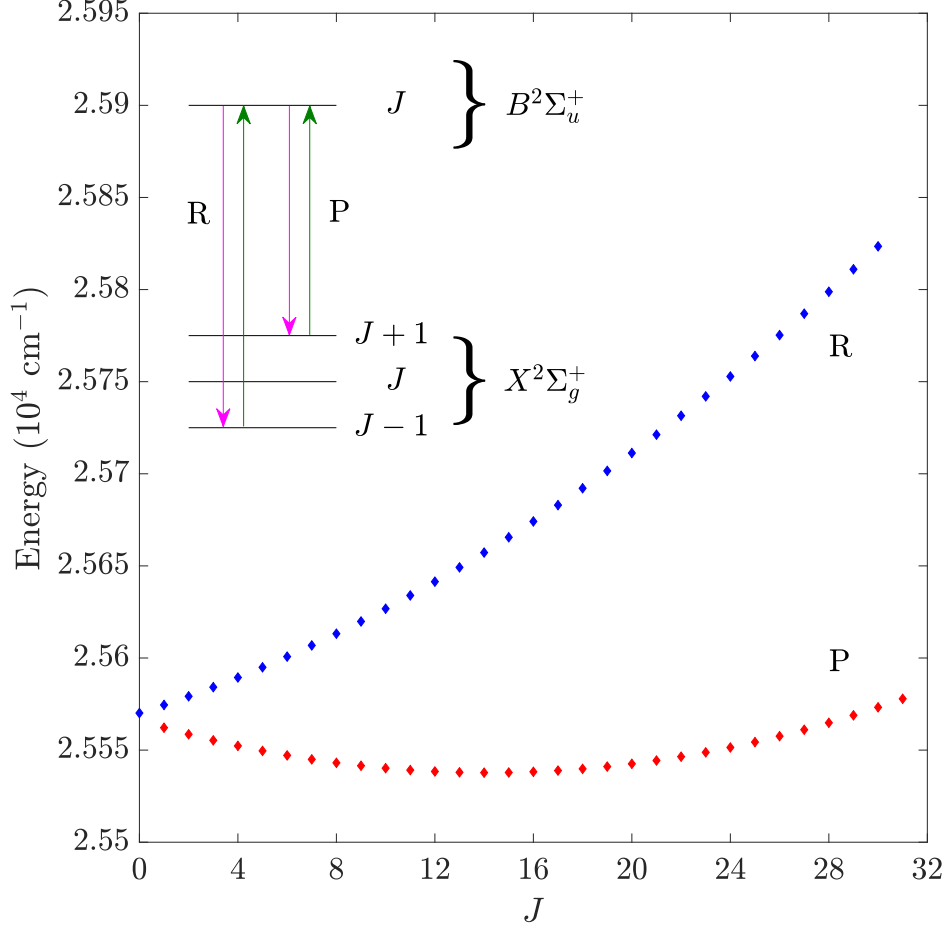


FIG. 1. Energy diagram of the P- and R-branches for radiative transitions $B^2\Sigma_u^+ \leftrightarrow X^2\Sigma_g^+$ in the vibrational ground state $v = 0$.

TABLE I. Molecular constants in cm^{-1} for the neutral ($X^1\Sigma_g^+$) and ionic states ($X^2\Sigma_g^+$ and $B^2\Sigma_u^+$) [31, 32].

State	B_e	D_e	β_e	ω_e	$X_e\omega_e$	$Y_e\omega_e$
$X^1\Sigma_g^+$ (N)	1.989581	$5.76 \cdot 10^{-6}$	(0)	(0)	(0)	(0)
$X^2\Sigma_g^+$ (X)	1.93176	$6.1 \cdot 10^{-6}$	0.01881	2207.00	16.10	-0.040
$B^2\Sigma_u^+$ (B)	2.07456	$6.17 \cdot 10^{-6}$	0.024	2419.84	23.18	-0.537

density $N_{mol} = 5 \times 10^{18} \text{ cm}^{-3}$. The rotational levels of the neutral are incoherently populated according to the Boltzmann distribution

$$\mathcal{P}_B(J, M) = \frac{g_J e^{-\varepsilon_J^N/kT}}{\sum_J g_J (2J+1) e^{-\varepsilon_J^N/kT}}, \quad (2)$$

where J is the total angular momentum of a particular N_2 molecule in the initial ensemble, and M is the projection of the angular momentum onto the z -axis of the laboratory frame, which is aligned along the polarization direction of the pump and the seed. The factor g_J takes into account the nuclear spin statistics [32], which for N_2 [4] is

$$g_J = \begin{cases} 2, & \text{for even } J \\ 1, & \text{for odd } J. \end{cases} \quad (3)$$

Note that in the initial thermal ensemble, the population of each J state is evenly distributed across its $M = 0, +1, \dots, +J$ sublevels.

Using linearly polarized pump and seed pulses, M is conserved throughout the dynamics due to cylindrical symmetry about the laser polarization direction. We therefore build a set of (J, J') -dependent density matrices, with one matrix for each group of initial rotational states with common quantum number $|M|$. The quantum dynamics are then computed separately for each $|M|$ -subset of states. In the following, we omit the M dependence of the density matrices, but wherever the summation over M is required, we will make it explicit in the equations.

The form that we adopt for the density matrix $\hat{\rho}^T(t)$ for the total system is

$$\hat{\rho}^T(t) = \hat{\rho}^N(t) + \hat{\rho}^I(t), \quad (4)$$

where

$$\hat{\rho}^N(t) = \sum_{JJ'} |N\rangle |JM\rangle \rho_{JJ'}^N(t) \langle J'M| \langle N| \quad (5)$$

is the density matrix for the neutral, and

$$\hat{\rho}^I(t) = \begin{bmatrix} \hat{\rho}^X(t) & \hat{\rho}^{XB}(t) \\ \hat{\rho}^{BX}(t) & \hat{\rho}^B(t) \end{bmatrix}, \quad (6)$$

is the density matrix of the ion that has been further split into the density matrices for the X and B states

$$\hat{\rho}^X(t) = \sum_{JJ'} |X\rangle |JM\rangle \rho_{JJ'}^X(t) \langle J'M| \langle X|, \quad (7a)$$

$$\hat{\rho}^B(t) = \sum_{JJ'} |B\rangle |JM\rangle \rho_{JJ'}^B(t) \langle J'M| \langle B|, \quad (7b)$$

and

$$\hat{\rho}^{XB}(t) = \sum_{JJ'} |X\rangle |JM\rangle \rho_{JJ'}^{XB}(t) \langle J'M | \langle B|, \quad (8a)$$

$$\hat{\rho}^{BX}(t) = \sum_{JJ'} |B\rangle |JM\rangle \rho_{JJ'}^{BX}(t) \langle J'M | \langle X| \quad (8b)$$

represent the coherences between the X and B electronic states. In Eqs. (5) to (8), $|JM\rangle$ are the standard spherical harmonic rotational functions $\langle \theta, \varphi | JM \rangle = Y_J^M(\theta, \varphi)$ with $\theta = 0$ corresponding to the same z -axis along which the laser pulses are polarized, $|N\rangle$ represents the electronic state of the neutral, and $|X\rangle$ and $|B\rangle$ represent the electronic states of the ion. With these definitions, the initial conditions at $t = 0$ become

$$\rho_{JJ'}^N(0) = \mathcal{P}_B(J, M) \delta_{JJ'} u[J - |M|] \quad (9a)$$

and

$$\rho_{JJ'}^X(0) = \rho_{JJ'}^B(0) = \rho_{JJ'}^{XB}(0) = \rho_{JJ'}^{BX}(0) = 0, \quad (9b)$$

where δ is the Kronecker delta, and u is the Heaviside discrete step function.

B. Pump stage

The pump laser pulse is defined as $\mathbf{E}_p(t) = \epsilon_z F_p(t) \cos(\omega_p t)$, with the envelope given by

$$F_p(t) = E_{p0} \begin{cases} \sin(\pi t / \tau_{on}), & 0 \leq t < \tau_{on} \\ 0, & t \geq \tau_{on} \end{cases} \quad (10)$$

and ϵ_z is the unit vector pointing along the z direction. This choice of $F_p(t)$ gives a “sin²” envelope for the intensity of the pump, where the full width at half maximum (FWHM) of the intensity profile is given by $\text{FWHM} = \tau_{on}/2$. We make the assumption that the pump pulse does not undergo significant change as it propagates through the medium, and hence there is no dependence of the equations used in the pump step along the propagation direction y .

The time evolution of the density matrices is described using the von Neumann equation, which in atomic units (a.u.) is

$$i \frac{\partial \hat{\rho}^k(t)}{\partial t} = [\hat{H}^k(t), \hat{\rho}^k(t)], \quad (11)$$

where $k = N, X, B, I$ represents the evolution equation for the neutral, X state, B state, and total ionic system respectively. The neutral Hamiltonian operator is

$$\hat{H}^N(t) = \sum_J \mathcal{E}_J^N |N\rangle |JM\rangle \langle JM| \langle N| + U(t, \theta) |N\rangle \langle N|, \quad (12)$$

where the first term on the left hand side is the rotational kinetic energy, and the second term is the interaction potential between the polarizability of the neutral molecule and pump laser field [1, 3, 33] with

$$U(t, \theta) = -\frac{1}{4}(\alpha_{\perp}^N + \Delta\alpha^N \cos^2 \theta) F_p^2(t). \quad (13)$$

In this last equation (13), θ is the angle between the internuclear axis and the laser polarization direction, and the polarizability anisotropy is $\Delta\alpha^N = \alpha_{\parallel}^N - \alpha_{\perp}^N$, where α_{\parallel}^N and α_{\perp}^N are the parallel and perpendicular elements of the polarizability tensor of the neutral (see Table II). In the $|JM\rangle$ basis, the Hamiltonian matrix for the neutral is composed of

$$\begin{aligned} H_{JJ'}^N(t) &= \langle JM | \hat{H}^N | J'M \rangle \\ &= (\mathcal{E}_J^N + U_{\perp}(t)) \delta_{JJ'} + U_0(t) R_{JJ'}, \end{aligned} \quad (14)$$

where

$$U_{\perp}(t) = -\alpha_{\perp}^N F_p^2(t)/4, \quad (15a)$$

$$U_0(t) = -\Delta\alpha^N F_p^2(t)/4, \quad (15b)$$

and $R_{JJ'}$ are the matrix elements of $\cos^2 \theta$

$$R_{JJ'} = \langle JM | \cos^2 \theta | J'M \rangle. \quad (16)$$

$R_{JJ'}$ are non-zero only if $J' = \{J-2, J, J+2\}$, allowing Raman transitions with $\Delta J = \pm 2$. Note that the $R_{JJ'}$ formally depend on M . In the following we will however omit their and all other matrix elements' M -dependence for clarity.

Due to the the exponential dependence of strong-field ionization on the instantaneous intensity of the driving laser pulse [34], we let ionization take place at the peak of the pump pulse at time $t = \tau_{on}/2$, which results in the population of the X and B ionic states. We construct the the ionic density matrices from the neutral density using the following steps.

First, we account for the angular dependence of the ionization probability $\mathcal{P}_I(\theta)$ estimating it as a ‘‘peanut’’ shape [35, 36]

$$\mathcal{P}_I(\theta) = \cos^2 \theta + \frac{1}{2}. \quad (17)$$

During the ionization step, the density that is transferred into the ionic states acquires this additional angular dependence. We take this into account by constructing an intermediate density matrix

$$\hat{\rho}' = \mathcal{C} \hat{Q} \hat{\rho}^N(\tau_{on}/2) \hat{Q}. \quad (18)$$

where the matrix elements of \hat{Q} are defined as

$$\begin{aligned} Q_{JJ'} &= \langle JM | \mathcal{P}_I(\theta) | J'M \rangle \\ &= R_{JJ'} + \frac{1}{2} \delta_{JJ'} u [J - |M|], \end{aligned} \quad (19)$$

with the same definitions for δ and u as in Eq. (9), and the normalization factor is

$$\mathcal{C} = \sum_M \text{tr}(\hat{\rho}^N(\tau_{on}/2)) / \sum_M \text{tr}(\hat{Q} \hat{\rho}^N(\tau_{on}/2) \hat{Q}), \quad (20)$$

where the summation over all the possible M -subsets in the initial thermal distribution is applied (recall Section II A for discussion about M -subsets). The inclusion of the normalization factor \mathcal{C} has the effect of preserving the norm of the total density matrix before and after the angular ionization probability $\mathcal{P}_I(\theta)$ is applied. This allows us to set the ionized fraction by using a scaling parameter η . We designate the fraction of N_2^+ ions with respect to neutrals as η , setting this value by hand. We also allow ourselves to vary the relative populations of the X and B states of the ion immediately after ionization, denoting these relative populations as p_X and p_B defined such that $p_X + p_B = 1$. Hence, ηp_X and ηp_B are the total populations in the X and B states.

Second, special consideration of the nuclear spin statistics must be taken [32]. While the electronic symmetry does not change during the $N \rightarrow X$ ionizing transition, it does during the $N \rightarrow B$ transition. This change in symmetry should be accompanied by a flip in the nuclear spin statistics $g_J \rightarrow g'_J$ where

$$g'_J = \begin{cases} 1, & \text{for even } J \\ 2, & \text{for odd } J. \end{cases} \quad (21)$$

In principle, if one would compute the ionization step with both the electronic and rotational degrees of freedom included rigorously and consistently, the only appearance of the nuclear spin factors would be in the initial Boltzmann distribution. For example, in one-photon ionization where the electronic and rotational degrees of freedom can be included on the same footing in first-order perturbation theory, the switch from g_J to g'_J occurs automatically

without needing to account for this flip by hand. In the case of strong-field ionization, however, a rigorous treatment of the ionization step that includes both the electronic and rotational degrees of freedom is not currently available, and we must account for the switch $g_J \rightarrow g'_J$ by hand during the $N \rightarrow B$ transition. This is accomplished when constructing $\hat{\rho}^B$ by i) dividing out the g_J factor from $\hat{\rho}'$, ii) multiplying in the g'_J . We label the resulting intermediate density matrix $\hat{\rho}''$.

With these steps in hand, the initial conditions for the density matrices in the ionic states that are populated by ionization at the peak of the pulse are then given by

$$\hat{\rho}^X(\tau_{on}/2) = \eta p_X \hat{\rho}', \quad (22)$$

$$\hat{\rho}^B(\tau_{on}/2) = \eta(1 - p_X) \hat{\rho}''. \quad (23)$$

The coherences between the X and B states remain zero during the ionization step

$$\rho_{JJ'}^{XB}(\tau_{on}/2) = \rho_{JJ'}^{BX}(\tau_{on}/2) = 0. \quad (24)$$

This is appropriate because, as mentioned above, we are considering the case where the emission must be seeded, which implies that there is no electronic coherence generated in the ion following ionization. From a physical point of view, the lack of coherence in the ion is due to the fact that the liberated electron is entangled with the ionic core, and tracing out the continuum electron degree of freedom decoheres the X and B ionic states.

For times $t \geq \tau_{on}/2$, $\hat{\rho}^X(t)$ and $\hat{\rho}^B(t)$ continue to evolve under the influence of the second half of the pump pulse and undergo further rotational excitation. This additional rotational excitation is included by solving the von Neumann equation (11) for the propagation of the coefficients $\rho_{JJ'}^X(t)$ and $\rho_{JJ'}^B(t)$. The $\hat{H}^X(t)$ and $\hat{H}^B(t)$ Hamiltonians used when solving Eq. (11) for the propagation of $\hat{\rho}^X(t)$ and $\hat{\rho}^B(t)$ have the analogous form to Eq. (14)

$$\hat{H}^X(t) = \sum_J \mathcal{E}_J^X |X\rangle |JM\rangle \langle JM| \langle X| + U(t, \theta) |X\rangle \langle X|, \quad (25a)$$

$$\hat{H}^B(t) = \sum_J \mathcal{E}_J^B |B\rangle |JM\rangle \langle JM| \langle B| + U(t, \theta) |B\rangle \langle B|, \quad (25b)$$

but with $U(t, \theta)$ now using the polarizabilities corresponding to the X and B states, see Table II.

After the pump is over, we continue the time evolution of the density matrices up until the seed pulse arrives using analytical solutions that have the same form for all three components

$$\hat{\rho}^k(t) = \hat{\rho}^k(\tau_{on}) \circ \Omega^k(t), \quad t > \tau_{on} \quad (26)$$

TABLE II. Polarizability coefficients calculated using the GAMESS electronic structure package [37], with the aug-cc-pVTZ basis set at a CAS MCSCF level of theory, evaluated at the equilibrium bondlength of the neutral.

State	$\Delta\alpha^k$ (a.u.)	α_{\perp}^k (a.u.)
$X^1\Sigma_g^+$ ($k = N$)	4.349	9.252
$X^2\Sigma_g^+$ ($k = X$)	9.695	8.509
$B^2\Sigma_u^+$ ($k = B$)	-4.68	6.582

for $k = N, X, B$, where the symbol \circ denotes the Hadamard product (element-wise matrix multiplication), and $\Omega^k(t)$ has the matrix elements

$$\Omega_{JJ'}^k(t) = \exp [i(\mathcal{E}_{J'}^k - \mathcal{E}_J^k)(t - \tau_{on})] \quad (27)$$

that depend on the differences of the energies in the corresponding electronic state.

Knowing the density matrices $\hat{\rho}^N(t)$, $\hat{\rho}^X(t)$ and $\hat{\rho}^B(t)$ then allows us to compute the alignment measures for all three components $k = \{N, X, B\}$

$$\langle \cos^2 \theta \rangle^k(t) = \frac{1}{p_k} \sum_M \text{tr}(\hat{\rho}^k(t) \hat{R}), \quad (28)$$

the \hat{R} operator has the matrix elements given in Eq. (16), and $p_N = 1$ since there is only one electronic state in the neutral that holds population. The $\langle \cos^2 \theta \rangle^k(t)$ quantities are commonly-used observables in the molecular alignment literature that allow us to follow the rotational wave-packet dynamics generated in the neutral and ion. In addition, these quantities will be used to construct the condition for gain outlined initially in Ref. [25].

The coherent rotations of the molecules generated by the pump pulse cause a time-dependent refractive index $n(t)$ defined by [33]

$$\begin{aligned} n^2(t) &= 1 + 4\pi N_{mol} \left[(1 - \eta) \alpha_{\perp}^N \right. \\ &\quad \left. + (1 - \eta) \Delta\alpha^N \langle \cos^2 \theta \rangle^N(t) \right] \\ &\equiv 1 + 4\pi N_{mol} \Theta_1(t). \end{aligned} \quad (29)$$

In principle there should be additional terms in Eq. (29) due to the rotational excitations in the ionic states, but these will have negligible contribution to $n(t)$ relative to the neutral terms as the fraction of ionized molecules η is assumed to be small. Eq. (29) is used below when propagating the seed pulse through the rotationally-excited medium.

C. Seed propagation

Our seed pulse is polarized along the z direction as the pump pulse, and is taken to propagate along the y direction through the medium. The initial seed pulse at the start of the medium ($y = 0$) is defined as

$$\mathbf{E}_s(t, y = 0) = \boldsymbol{\epsilon}_z E_s(t, y = 0), \quad (30)$$

with

$$E_s(t, y = 0) = E_{s0} e^{-4 \log 2 \left(\frac{t - t_{del}}{\sigma_s} \right)^2} \cos(\omega_s(t - t_{del})), \quad (31)$$

where σ_s is the full width at the half-maximum of the seed envelope, ω_s is the central frequency of the seed, and t_{del} is the delay time of the seed pulse.

Qualitatively, the time evolution of $E_s(t, y)$ proceeds as follows. With the seed pulse defined for all time at the entrance of the medium by Eq. (31), we first compute the response of the medium by using $E_s(t, y = 0)$ in a von Neumann equation for $\hat{\rho}^I(t, y = 0)$ that couples the X and B states through the dipole interaction, using the $\hat{\rho}^X(t)$ and $\hat{\rho}^B(t)$ computed in the pump section as initial conditions for $\hat{\rho}^I(t, y = 0)$. Second, once $\hat{\rho}^I(t, y = 0)$ is calculated following the interaction with the seed pulse, we use this $\hat{\rho}^I(t, y = 0)$ to compute the polarization of the medium which is then used as input into the Maxwell wave equation to propagate $E_s(t, y = 0)$ to the next spatial point along y . These two steps are then repeated to continue propagating the seed pulse through the medium, with $E_s(t, y = 0)$ replaced with $E_s(t, y)$ at the current y position. We now outline the equations used in these two steps to compute $\hat{\rho}^I(t, y)$ and to propagate $E_s(t, y)$ along the y -direction.

The initial ionic density matrix for any y -coordinate is constructed as

$$\hat{\rho}^I(t = t_s, y = 0) = \begin{bmatrix} \hat{\rho}^X(t_s) & \emptyset \\ \emptyset & \hat{\rho}^B(t_s) \end{bmatrix}, \quad (32)$$

and where \emptyset is a zero matrix. The time $t = t_s$ is some point in time after the pump pulse is over where we wish to start the time evolution of the seed pulse. The evolution of $\hat{\rho}^I(t, y = 0)$ for time $t > t_s$ is carried out by solving the von Neumann equation (11). The ionic Hamiltonian $\hat{H}^I(t, y)$ is written as

$$\hat{H}^I(t, y) = \begin{bmatrix} \hat{H}^X & \hat{H}^{XB}(t, y) \\ \hat{H}^{BX}(t, y) & \hat{H}^B \end{bmatrix}, \quad (33)$$

where

$$\hat{H}^{XB}(t, y) = (\hat{H}^{BX}(t, y))^\dagger = -\boldsymbol{\mu} \cdot \mathbf{E}_s(t, y) \quad (34)$$

accounts for the interaction between the weak resonant seed pulse and the ionic states. Because the seed is assumed to be in the weak-field limit, the off-resonant polarizability interaction analogous to $U(t, \theta)$ from Eq. (13) that would be induced by the seed pulse is now negligible, so that Eqs. (25) become

$$\hat{H}^X = \sum_J \mathcal{E}_J^X |X\rangle \langle JM| \langle JM| \langle X|, \quad (35a)$$

$$\hat{H}^B = \sum_J \mathcal{E}_J^B |B\rangle \langle JM| \langle JM| \langle B|, \quad (35b)$$

during the seed step. The energies \mathcal{E}_J^X and \mathcal{E}_J^B are computed according to Eq. (1) for $v = 0$ corresponding to the 391 nm transition in N_2^+ . The B - X dipole coupling is a parallel transition, in which case the dipole interaction reduces to

$$-\boldsymbol{\mu} \cdot \mathbf{E}_s(t, y) = -\mu_{XB} E_s(t, y) \cos \theta, \quad (36)$$

where the transition dipole $\mu_{XB} = -0.74$ a.u. was computed with GAMESS using the same level of electronic structure used to compute the polarizabilities above. $\hat{H}^{XB}(t, y)$ can then be written as

$$\hat{H}^{XB}(t, y) = -\mu_{XB} E_s(t, y) \hat{S}, \quad (37)$$

where the matrix elements of \hat{S} are given by

$$S_{JJ'} = \langle JM | \cos \theta | J'M \rangle. \quad (38)$$

The only non-zero $S_{JJ'}$ occur when $J - J' = \pm 1$, resulting in the expected one-photon selection rules for the transitions between rotational levels of the B and X states. Note that $\hat{H}^{XB}(t, y)$ will generate coherences between the X and B electronic states of the ion that in turn cause absorption and/or emission at the $X \leftrightarrow B$ transition frequencies.

After computing $\hat{\rho}^I(t, y)$, which describes the microscopic properties of the medium, we can calculate the macroscopic polarization $P_\mu(t, y)$ of the medium induced by the seed pulse along $\boldsymbol{\epsilon}_z$

$$\begin{aligned} P_\mu(t, y) &= \eta N_{mol} \langle \boldsymbol{\mu} \cdot \boldsymbol{\epsilon}_z \rangle \\ &= \eta N_{mol} \langle \mu_{XB} \cos \theta \rangle \\ &= \eta N_{mol} \mu_{XB} \sum_M \text{tr}(\hat{\rho}^I(t, y) \mathbb{S}), \end{aligned} \quad (39)$$

where the transition matrix \mathbb{S} has the form

$$\mathbb{S} = \begin{bmatrix} \emptyset & \hat{S} \\ \hat{S} & \emptyset \end{bmatrix}. \quad (40)$$

Also recall that at the pump stage, the excited rotation of the molecules generates a time-dependent refractive index given by Eq. (29). When the seed pulse propagates in the rotationally-excited medium, it is also affected by this refractive index giving rise to an additional contribution to the macroscopic polarization of the medium seen by the seed pulse given by

$$P_{N_2}(t) = N_{mol}E_s(t, y)\Theta_1(t), \quad (41)$$

where $\Theta_1(t)$ is defined by Eq. (29). Due to the fact that we restrict ourselves to small values of η (i.e. small fraction of ionized molecules), $n(t)$ is effectively the time-dependent refractive index generated by the rotationally-excited neutral molecules, and hence we have labeled the associated polarization in Eq. (41) as P_{N_2} to indicate that this polarization comes from the neutral N_2 .

We compute the propagation of the electric field $E_s(t, y)$ of the seed using a simplified Maxwell wave equation [38]

$$\frac{\partial E_s(t, y)}{\partial y} + \frac{1}{c} \frac{\partial E_s(t, y)}{\partial t} = -\frac{2\pi}{c} \frac{\partial P(t, y)}{\partial t}, \quad (42)$$

where the polarization $P(t, y)$ consists of the two terms introduced above

$$P(t, y) = P_{N_2}(t) + P_\mu(t, y). \quad (43)$$

Eq. (42) is derived by including only the forward propagating waves, and is equivalent to the slowly-varying envelope approximation in the limit of long pulse durations [33]. We solve Eq. (42) in a reference frame that is moving at roughly the average velocity of the pump pulse by introducing the new variable $\tau = t - y/v_p$, where the velocity of this moving frame is taken to be

$$v_p = c \left\{ 1 + 2\pi N_{mol} \left[(1 - \eta)(\alpha_\perp^N + \Delta\alpha^N/3) + \eta p_X(\alpha_\perp^X + \Delta\alpha^X/3) + \eta p_B(\alpha_\perp^B + \Delta\alpha^B/3) \right] \right\}^{-1}. \quad (44)$$

Eq. (42) can then be written as

$$\frac{\partial E_s(\tau, y)}{\partial y} = \frac{1}{v_r} \frac{\partial E_s(\tau, y)}{\partial \tau} - \frac{2\pi}{c} \frac{\partial P(\tau, y)}{\partial \tau}, \quad (45)$$

where $v_r = cv_p/(c - v_p)$.

The gain and/or absorption of the seed pulse is computed as the ratio of the integrated spectral intensities after propagating in the rotationally excited medium and the intensity before the interaction. Specifically, we calculate

$$\Gamma(t_{del}, z_{max}) = 1 + \frac{\int_{\omega_P}^{\omega_R} [I_{out}(\omega, t_{del}, z_{max}) - I_{in}(\omega)] d\omega}{\int_{\omega_P}^{\omega_R} I_{in}(\omega) d\omega}, \quad (46)$$

where I_{in} and I_{out} are the spectral intensities (i.e Fourier power spectrum) of the seed pulse at the input and output of the medium respectively, ω_P is the minimum of the P-branch parabola (see Fig. 1), and ω_R corresponds to the maximal transition in the R-branch under consideration. When $\Gamma > 1$ the seed has undergone gain, while $\Gamma < 1$ implies that absorption rather than gain of the seed has occurred.

D. Numerical Considerations

We numerically solve the von Neumann equation Eq. (11) using the Runge-Kutta fourth order (RK4) scheme [39] to obtain the time evolution of the coefficients $\rho_{JJ'}^N(t)$ of the neutral density matrix. For the pump step, our RK4 propagation used a time step of $\Delta t = 1$ fs. The maximum number of the rotational states was set to $J_{max} = 40$ in both the seed and pump steps, and the maximum rotational number used to average over the initial thermal distribution of the neutral N₂ was $J_{max0} = 30$.

Efficient propagation during the seed step requires further care due to the disparate timescales imposed by the electronic energy separation of the X and B states. We first write the density matrix elements in terms of slowly-varying amplitudes $A_{JJ'}^k(t)$,

$$\rho_{JJ'}^k(t) = A_{JJ'}^k(t) e^{i(\mathcal{E}_{J'}^k - \mathcal{E}_J^k)t} \quad (47a)$$

for $k = X, B$, and

$$\rho_{JJ'}^{XB}(t) = A_{JJ'}^{XB}(t) e^{i(\mathcal{E}_{J'}^B - \mathcal{E}_J^X)t}, \quad (47b)$$

$$\rho_{JJ'}^{BX}(t) = A_{JJ'}^{BX}(t) e^{i(\mathcal{E}_{J'}^X - \mathcal{E}_J^B)t}. \quad (47c)$$

Similarly, we write the electric field of the seed as

$$E_s(t, y) = F_s(t, y) e^{i\omega_s t} + F_s^*(t, y) e^{-i\omega_s t}. \quad (48)$$

This approach has the advantage of analytically incorporating the fast oscillations related to the electronic spacing and the seed carrier wave into the numerical propagation scheme. We proceed to apply the RK4 method to the von Neumann propagation of the $A_{JJ'}^k(t)$, $A_{JJ'}^{XB}(t)$, and $A_{JJ'}^{BX}(t)$ with a time step of 0.305 fs. For the spatial propagation of $F_s(t, y)$, we implement the Lax-Wendroff method leading to a 2^{nd} order numerical scheme [39, 40] with CFL-number $\Lambda = \Delta y / (v_r \Delta t) = 0.99$, where $\Delta y = 2.8 \times 10^{-2}$ mm and $\Delta t = 0.00477$ fs are the space and time steps used in the seed pulse propagation iterations. The slowly-varying density matrix elements are converted from the coarse time grid used in the von Neumann step to the fine time grid used in the Lax-Wendroff step using spline interpolation. To use the RK4 scheme in propagating the ionic density matrix elements, we need to know not only $F_s(t_n, y_k)$ and $F_s(t_{n+1}, y_k)$, where t_n and t_{n+1} are two neighboring time points at the k^{th} spatial coordinate y_k , but also the intermediate values $F_s(t_n + \Delta t/2, y_k)$. To preserve the 4^{th} order of RK4 we use the 4^{th} order Lagrange approximation for these intermediate points.

E. Perturbative Treatment of Seed- N_2^+ interaction

In Ref.[25], it was suggested that the gain seen in N_2^+ lasing should be related to the molecular alignment in X and B . In particular, it was proposed that the gain of the delayed seed pulse should be proportional to the difference of the alignment in the X and B states at the moment $t = t_{del}$ when the seed arrives

$$W_{down \leftrightarrow up}(t_{del}) = p_B \langle \cos \theta \rangle^B(t_{del}) - p_X \langle \cos \theta \rangle^X(t_{del}). \quad (49)$$

Note that unlike Γ defined in Eq. (46), the estimate $W_{down \leftrightarrow up}$ predicts gain when $W_{down \leftrightarrow up} > 0$, while absorption corresponds to $W_{down \leftrightarrow up} < 0$. In this section, we apply first-order perturbation theory to the interaction between the weak seed pulse and the rotationally-excited medium, and demonstrate how to recover the condition for gain in Eq. (49). Understanding the conditions required to recover the $W_{down \leftrightarrow up}$ estimate will help us to understand the cases presented below where the fully-numerical formalism starts to diverge from this estimate. We apply the perturbation theory within the wavefunction formalism, which allows us to obtain the perturbative result in the clearest way.

The wave function for a generic rotationally-excited wave packet in the ion after the pump pulse can be written as

$$|\Psi(t)\rangle = \sum_J x_J^{(0)} e^{-i\mathcal{E}_J^X t} |X\rangle |JM\rangle \quad (50)$$

$$+ \sum_{J'} b_{J'}^{(0)} e^{-i\mathcal{E}_{J'}^B t} |B\rangle |J'M\rangle, \quad (51)$$

where we have labeled the amplitudes of the wave function with a superscript '(0)' to imply that they are the zeroth-order amplitudes (i.e. they do not contain any interaction with the seed pulse.)

Consider first the process of absorption by a seed pulse that arrives at time t_{del} . Absorption physically corresponds to moving population from X to B , and we therefore compute the first-order corrections to the amplitudes in B that arise from seed-driven transitions from X to B

$$b_J^{(1)}(t_{del}) = i\mu_{XB} \left[\mathcal{F}(\omega_{JJ-1}^{BX}) S_{JJ-1} x_{J-1}^{(0)} e^{i\omega_{JJ-1}^{BX} t_{del}} + \mathcal{F}(\omega_{JJ+1}^{BX}) S_{JJ+1} x_{J+1}^{(0)} e^{i\omega_{JJ+1}^{BX} t_{del}} \right], \quad (52)$$

where $\omega_{JJ'}^{BX} = (\mathcal{E}_J^B - \mathcal{E}_{J'}^X)$ are the transition frequencies, $\mathcal{F}(\omega_{JJ'}^{BX})$ are the Fourier amplitudes of the seed pulse at these frequencies, and $S_{JJ'} = \langle JM | \cos\theta | J'M \rangle$ as was defined in Eq. (38). Since the $b_J^{(1)}$ are the excited state amplitudes generated by the seed, the total absorption can be estimated by summing over all the first-order B populations:

$$\sum_J |b_J^{(1)}(t_{del})|^2 = |\mu_{XB}|^2 \sum_J \left[|\mathcal{F}(\omega_{JJ-1}^{BX})|^2 |S_{JJ-1}|^2 |x_{J-1}^{(0)}|^2 + |\mathcal{F}(\omega_{JJ+1}^{BX})|^2 |S_{JJ+1}|^2 |x_{J+1}^{(0)}|^2 \right. \\ \left. + 2\mathcal{F}(\omega_{JJ-1}^{BX})^* \mathcal{F}(\omega_{JJ+1}^{BX}) S_{JJ-1} S_{JJ+1} x_{J-1}^{(0)*} x_{J+1}^{(0)} \cos([\mathcal{E}_{J+1}^X - \mathcal{E}_{J-1}^X] t_{del}) \right]. \quad (53)$$

In order to eventually recover the $W_{down \leftrightarrow up}$ estimate, we must now make the assumption that the bandwidth is flat across all transition frequencies: $\mathcal{F}(\omega_{JJ'}^{BX}) = \text{constant}$ for all $\omega_{JJ'}^{BX}$.

For convenience, we choose to set $\mathcal{F}(\omega_{JJ'}^{BX}) = 1$. This gives

$$\sum_J |b_J^{(1)}(t_{del})|^2 = |\mu_{XB}|^2 \sum_J \left[(|S_{J+1,J}|^2 + |S_{J-1,J}|^2) |x_J^{(0)}|^2 \right. \\ \left. + 2S_{J+1,J} S_{J+2,J+1} x_J^{(0)*} x_{J+2}^{(0)} \cos([\mathcal{E}_{J+2}^X - \mathcal{E}_J^X] t_{del}) \right], \quad (54)$$

where we have also taken the liberty of rearranging some of the indices in the summation.

With a little algebra, Eq. (54) can be seen to be equivalent to the expression

$$\sum_J |b_J^{(1)}(t_{del})|^2 = p_X |\mu_{XB}|^2 \langle \cos^2 \theta \rangle^X(t_{del}) \quad (55)$$

where $\langle \dots \rangle^X(t_{del})$ means that we are taking the expectation value of the rotational wave packet over the zeroth-order X state at the time t_{del} , and the appearance of the population term p_X accounts for the fact that the population in the X state is not unity. In going from Eq. (54) to (55) we have made use of the fact that $(|S_{J+1,J}|^2 + |S_{J-1,J}|^2) = R_{JJ}$ and $S_{J+1,J}S_{J+1,J+2} = R_{JJ+2}$, where the $R_{JJ'}$ are the matrix elements of $\cos^2 \theta$ defined in Eq. (16). These two properties can be derived from the properties of spherical harmonics.

Equation (55) shows that the absorption from the X state is proportional to the alignment in the X state. A corresponding expression for the emission from the state B can be analogously derived by repeating the steps that lead from Eq. (52) to (55) but now considering the first-order corrections to the X state that account for the seed-driven transitions from B to X . This calculation yields

$$\sum_J |x_J^{(1)}(t_{del})|^2 = p_B |\mu_{XB}|^2 \langle \cos^2 \theta \rangle^B(t_{del}), \quad (56)$$

which shows that the emission from B is proportional to the alignment in the B state. The total expected emission from the system, which would be given by the emission from B minus the absorption from X , can be now constructed by combining the expressions (55) and (56)

$$\begin{aligned} \sum_J |x_J^{(1)}(t_{del})|^2 - \sum_J |b_J^{(1)}(t_{del})|^2 &= |\mu_{XB}|^2 \left(p_B \langle \cos^2 \theta \rangle^B(t_{del}) - p_X \langle \cos^2 \theta \rangle^X(t_{del}) \right) \\ &\equiv |\mu_{XB}|^2 W_{down \leftrightarrow up}(t_{del}), \end{aligned} \quad (57)$$

which gives the gain estimate Eq. (49) proposed in Ref.[25]. Since $W_{down \leftrightarrow up}$ is constructed to reflect the emission minus the absorption, a value of $W_{down \leftrightarrow up} > 0$ predicts gain while $W_{down \leftrightarrow up} < 0$ predicts absorption. Although this result was here derived using a single wave function, the same result is obtained using perturbation theory in the density matrix approach, and the result still holds when averaging over an initial thermal distribution. Further, it should be stressed that obtaining the expression for $W_{down \leftrightarrow up}$ required that we assume a flat bandwidth. This point will be important below to understand cases where the gain starts to diverge from the estimate $W_{down \leftrightarrow up}$.

III. RESULTS AND DISCUSSION

A. Rotational excitation and wave packet dynamics

We first discuss the rotational excitation and rotational wave packets generated in the pump step. The initial thermal rotational distribution of the neutral at temperature $T = 298$ K is plotted in Fig. 2a, while Figs. 2b and c show examples of the rotational distributions in the X and B ionic states after the pump pulse has past. For these cases, we used a peak pump intensity of $I_{pump} = 1 \times 10^{14}$ W/cm² (Fig. 2b) and $I_{pump} = 2 \times 10^{14}$ W/cm² (Fig. 2c), the duration of the pump pulse was $\tau_{on} = 50$ fs (FWHM = 25 fs), and the number density was $N_{mol} = 5 \times 10^{18}$ cm⁻³. The relative ionic populations were set to $p_X = 0.45$ and $p_B = 0.55$.

Figures 2b and c show that both the X and B ionic states are rotationally hotter than the initial neutral thermal distribution, reflecting the rotational excitation imparted by the pump pulse. In addition, we find that the X state is rotationally hotter than the B state, an effect that is more pronounced in the $I_{pump} = 2 \times 10^{14}$ W/cm² case (Fig. 2c). This difference between the X and B states is due to the different polarizabilities for the X and B states, $\Delta\alpha^X$ and $\Delta\alpha^B$. In the first half of the pump pulse, the neutral receives a torque toward the pump polarization direction (the z -axis in our case). Following ionization, the population in X continues to receive additional torque toward the z -axis. However, the population in the B state receives a torque in the opposite direction since $\Delta\alpha^B$ has the opposite sign compared to $\Delta\alpha^N$ and $\Delta\alpha^X$, and hence the torque received on the second half of the pump pulse for the B state is partially undoing the rotational excitation imparted to the neutral on the first half of the pump pulse.

Figures 3a and b plot the alignment measure $\langle \cos^2 \theta \rangle(t)$ for the neutral and ionic states after the pump pulse, again for $I_{pump} = 1 \times 10^{14}$ W/cm² (Fig. 3a) and $I_{pump} = 2 \times 10^{14}$ W/cm² (Fig. 3b), which shows the coherent rotational dynamics that occurs following the pump pulse. Qualitatively, a large value of $\langle \cos^2 \theta \rangle(t)$ means that the molecules are preferentially aligned along the pump polarization direction, while a smaller value of the alignment parameter implies that the molecules are more aligned perpendicular to this direction. The revivals for the different states have different timings, which is due primarily to the different rotational energy constant B_e of each state.

B. Modulation of the seed gain

We now consider the seed propagation. Fig. 4a shows the spectrum of the initial seed pulse at the entrance to the medium, while Fig. 4b shows an example of the output seed spectrum. The input seed pulse had a peak intensity of $I_{seed} = 10^{11}$ W/cm², a duration of $\sigma_s = 20$ fs, a central wavelength of $\lambda_s = 391$ nm, and a total propagation length of $z_{max} = 0.5$ mm was used. The example case in Fig. 4 corresponds to a delay of $t_{del} = 5$ ps, and the relative ionic populations were set to $p_X = 0.45$ and $p_B = 0.55$, and the fraction of ionized molecules was set to $\eta = 0.001$ (i.e. 0.1%). The pump intensity used was $I_{pump} = 10^{14}$ W/cm². As can be seen in the figure, the output spectrum of the seed pulse has developed gain and absorption structures in the energy region of the rotational transitions. The Γ parameter in Eq. (46) is computed by integrating across this gain/absorption window.

Figure 5 shows various cases of the total gain and absorption as a function of the seed delay t_{del} . The left column corresponds to $p_X = 0.45$ and $p_B = 0.55$ where electronic inversion is present, while the right column corresponds to $p_X = 0.55$ and $p_B = 0.45$ where electronic inversion is absent. All other parameters are the same as used in Fig.4. The top row of Figure 5 plots the perturbative estimate $W_{down\leftrightarrow up}$, while the following rows plot the Γ parameter computed from the full numerical propagation of the seed, for various values of the ionization fraction η which are labeled on the plots.

The $W_{down\leftrightarrow up}$ curves shown in Figure 5 show that the expected gain and absorption is modulated as the rotational wave packets on X and B evolve and modulate the $\langle \cos^2 \theta \rangle^{X,B}(t_{del})$ parameters that enter into the $W_{down\leftrightarrow up}$ estimate. Importantly, one can see that in both cases of inversion (left) or no inversion (right) the behavior of the emission can switch from gain to absorption and back depending on the particular delay chosen to launch the seed pulse. Regarding the results for the full seed propagation, we can see that in the case of $\eta = 0.1\%$ (low ionization) the numerically-calculated gain Γ almost exactly mirrors the predictions of the $W_{down\leftrightarrow up}$ estimate; when $W_{down\leftrightarrow up} > 0$ gain is predicted and correspondingly the results of the numerical propagation of the seed yield $\Gamma > 1$. We emphasize that these results demonstrate that gain can be achieved in the absence of electronic inversion when there are rotational coherences present that can modulate the balance between emission and absorption in the system.

In the cases of $\eta = 1\%$ and 3% also shown in Fig.5, we see that Γ starts to diverge from

the $W_{down\leftrightarrow up}$ estimate. This occurs because in these cases the density of the ions is large enough to generate substantial gain in the seed, and as the amplitudes of the gain lines in the seed spectrum increase the assumption of a flat spectrum required to derive $W_{down\leftrightarrow up}$ no longer holds. The increased strength of the gain, and hence the increased amplitude of the corresponding gain lines, is evidenced by the fact that Γ reaches a maximum of about 1.02 in the $\eta = 0.1\%$ case while it shoots up to about 1.38 and 2.9 in the $\eta = 1\%$ and 3% cases respectively. Recall that due to the definition of Γ given in Eq. (46), a value close to 1 implies a small change in total intensity of the seed pulse, while a larger value like 2.9 implies a rise in intensity of that same amount at the $B \leftrightarrow X$ transition frequencies. Deviations of Γ away from $W_{down\leftrightarrow up}$ would equivalently occur in the case of $\eta = 0.1\%$ if the propagation length is increased; as the propagation length increases so will the amplitudes of the gain lines, which in turn will cause a breakdown of the flat spectrum approximation. Qualitatively, the deviations away from $W_{down\leftrightarrow up}$ in the large gain regime appear as an increased amount of oscillations in Γ compared to what one would expect from the behaviors of $\langle \cos^2 \theta \rangle^X(t)$ and $\langle \cos^2 \theta \rangle^B(t)$ alone. These increased oscillations in the delay-dependent gain of a seed pulse have been observed in recent experiments [24].

Figure 6 shows additional results of the modulation of the gain for the hypothetical cases where only one of the two ionic states was rotationally pumped. In Fig.6a, we only generated a rotational wave packet in the B state while forcing the population in X to be in a thermal distribution of rotational states at $T=298$ K. The relative ionic populations were set to $p_X = 0.55$ and $p_B = 0.45$ (i.e. no electronic inversion) and $\eta = 0.1\%$ was used. There remain values of the delay where gain ($\Gamma > 1$) is achieved. Fig.6b, shows the analogous case where we have kept the coherent rotational excitations in X while replacing the B state with a thermal distribution. Again we can see delays where gain occurs. These simulations show that it is enough to have rotational coherences in only one of the participating electronic states in order to generate gain without inversion.

Finally, we consider the Fourier spectrum of the delay-dependent gain signal. It can be shown that, for linear molecules, the alignment parameter $\langle \cos^2 \theta \rangle(t)$ contains the frequencies

$$\omega_J = \mathcal{E}_{J+2} - \mathcal{E}_J \approx B(4J + 6), \quad (58)$$

where B is the rotational constant of the molecule being considered [4]. In the low gain regime, we have seen that the delay-dependent emission/absorption temporally follows the

formula in Eq. (49) and hence we expect the Fourier transform of the gain/absorption to contain two series of peaks like in Eq. (58), one reflecting the rotational spacings of X and the other reflecting the rotational spacings of B . Fig.7 shows the Fourier transform for two of the absorption/gain signals $\Gamma(t_{del})$ presented in Fig. 5, one in the low-gain regime ($\eta = 0.1\%$) and the second for the high-gain regime ($\eta = 3\%$). In the low-gain regime ($\eta = 0.1\%$), two series of peaks in the Fourier spectrum can be seen, and they line up perfectly with the expected frequencies $\omega_j^k = \mathcal{E}_{j+2}^k - \mathcal{E}_j^k$ ($k = X, B$) for the X and B states. However, once the gain becomes larger and the delay-dependent emission diverges from the $W_{down\leftrightarrow up}$ estimate, new frequencies that are not accounted for by these ω_j^k arise. This can be seen in the $\eta = 3\%$ case in Fig.7; new frequencies that do not align with ω_j^k are now present. These new frequencies are a result of the interplay between the timescales required for the gain lines to grow substantially in amplitude and the timescales of the coherent rotational wave packet.

C. Structure of the spectra

Figures 8 and 9 present a more detailed view of the gain and absorption lines in the output seed pulse. Both figures plot a scaled logarithm of the change in the output and input spectrum of the seed defined by

$$\Delta I_{\log} = \log_{10} \left(\frac{\Delta I(\omega) + \Delta I_{min} + \Delta I_{max}}{\Delta I_{min} + \Delta I_{max}} \right) \quad (59)$$

where $\Delta I(\omega) = I_{out}(\omega) - I_{in}(\omega)$ is the difference between the output and input spectral intensities of the seed, and ΔI_{min} and ΔI_{max} are the minimum and maximum of $\Delta I(\omega)$ respectively. The range of energies plotted corresponds to the energy window of the $B \leftrightarrow X$ transitions. With the definition in Eq (59), $\Delta I_{\log} > 0$ represents gain, while $\Delta I_{\log} < 0$ corresponds to absorption. All simulation parameters are the same as used in Fig.5 with $\eta = 0.1\%$, $p_X = 0.45$ and $p_B = 0.55$. Fig.8 shows ΔI_{\log} for the specific delay of $t_{del} = 4.3$ ps, while Fig. 9 shows ΔI_{\log} for a range of delays; Fig. 8 is a slice through Fig. 9 at the delay $t_{del} = 4.3$ ps. The 2D spectrum in Fig. 9 exhibits a rich modulation structure that is a result of the underlying rotational coherences comprising the rotational wave packets. These structures and modulations are in excellent agreement with those found experimentally in high-resolution measurements of the delay-dependent seeded N_2^+ lasing as

can be seen by comparing against Fig.1 from Ref.[22], which confirms that our model is capturing the essential effects of the rotational coherences on the gain and absorption of the delayed seed pulse. One final comment regarding the spectrum in Fig. 9 relates to the subtle vertical features that appear near 4, 8, and 12 ps. These features are caused by the time-dependent refractive index of the neutral rotational wavepackets [Eqs. (29) and (41)]. Similar modulations appearing at the revival times of the neutral rotational wavepackets have also been observed, and these modulations caused by the time-dependent refractive index of the neutral were experimentally found to persist long after the ion-driven rotational modulations of the gain have decayed away [22].

IV. CONCLUSION

Motivated by the seeded version of ultrafast N_2^+ lasing, we have developed and explored a coupled Maxwell/von Neumann model that simulates the propagation of a seed pulse in an ionized and rotationally-excited gas of N_2 molecules. The model is aimed at understanding how the presence of rotational wavepackets modulates the absorption and gain of a delayed seed pulse and expands on the idea of transient inversion in rotationally-aligned nitrogen first discussed in Ref.[25]. Our numerical results successfully capture experimentally-observed modulations [17, 22, 24] of delay-dependent gain properties driven by the coherent rotational excitations. Using first-order time-dependent perturbation theory, we show that the gain estimate $W_{down\leftrightarrow up}$ suggested in Ref.[25] correctly captures the rotational modulations of the gain/absorption in the limit of low gain and absorption. As the total gain increases, the numerically-calculated rotationally-driven modulations of the gain start to diverge from the $W_{down\leftrightarrow up}$ estimate. This divergent behavior occurs due to the non-flat structure of the seed spectrum that results from the growth of the gain lines at the $B \leftrightarrow X$ transition frequencies. Finally, we have demonstrated that gain in the absence of electronic inversion is possible in N_2^+ lasing due to the presence of rotational coherence.

V. ACKNOWLEDGMENTS

We thank Paul Corkum, Ladan Arissian, Mathew Britton, and David Villeneuve for numerous stimulating discussion regarding N_2^+ lasing. M.S. acknowledges the financial support

from the Natural Science and Engineering Research Council (NSERC) of Canada through their Discovery Grants program.

- [1] B. Friedrich and D. Herschbach, *Phys. Rev. Lett.* **74**, 4623 (1995).
- [2] J. Larsen, I. Wendt-Larsen, and H. Stapelfeldt, *Phys. Rev. Lett.* **83**, 1123 (1999).
- [3] H. Stapelfeldt and T. Seideman, *Rev. Mod. Phys.* **75**, 543 (2003).
- [4] P. W. Dooley, I. V. Litvinyuk, K. F. Lee, D. M. Rayner, M. Spanner, D. M. Villeneuve, and P. B. Corkum, *Phys. Rev. A* **68**, 234061 (2003).
- [5] T. Seideman, *Phys. Rev. Lett.* **83**, 4971 (1999).
- [6] J. Ortigoso, M. Rodriguez, M. Gupta, and B. Friedrich, *J. Chem. Phys.* **110**, 3870 (1999).
- [7] F. Rosca-Pruna and M. Vrakking, *Phys. Rev. Lett.* **87**, 153902 (2001).
- [8] J. Eberly, N. Narozhny, and J. Sanchez-Mondragon, *Phys. Rev. Lett.* **44**, 1323 (1980).
- [9] I. Averbukh and N. Perelman, *Phys. Lett. A* **139**, 449 (1989).
- [10] V. Kalosha, M. Spanner, J. Herrmann, and M. Ivanov, *Phys. Rev. Lett.* **88**, 103901 (2002).
- [11] R. Bartels, T. Weinacht, N. Wagner, M. Baertschy, C. Greene, M. Murnane, and H. Kapteyn, *Phys. Rev. Lett.* **88**, 2002 (2002).
- [12] G. S. Thekkadath, K. Heshami, D. G. England, P. J. Bustard, B. J. Sussman, and M. Spanner, *J. Mod. Opt.* **63**, 2093 (2016).
- [13] Q. Luo, W. Liu, and S. Chin, *App. Phys. B* **76**, 337 (2003).
- [14] J. Yao, B. Zeng, H. Xu, G. Li, W. Chu, J. Ni, H. Zhang, S. Chin, Y. Cheng, and Z. Xu, *Rhys. Rev. A* **84**, 051802(R) (2011).
- [15] Y. Liu, Y. Brelet, G. Point, A. Houard, and Mysyrowicz, *Opt. Exp.* **21**, 22792 (2013).
- [16] J. Ni, W. Chu, C. Jing, H. Zhang, B. Zeng, J. Yao, G. Li, H. Xie, C. Zhang, H. Xu, S. Chin, Y. Cheng, and Z. Xu, *Opt. Express* **21**, 8746 (2013).
- [17] H. Zhang, C. Jing, J. Yao, G. Li, B. Zeng, W. Chu, J. Ni, H. Xie, H. Xu, S. Chin, K. Yamanouchi, Y. Cheng, and Z. Xu, *Phys. Rev. X* **3**, 041009 (2013).
- [18] B. Zeng, W. Chu, G. Li, J. Yao, H. Zhang, J. Ni, C. Jing, H. Xie, and Y. Cheng, *Phys. Rev. A* **89**, 042508 (2014).
- [19] H. Xu, E. Ltstedt, A. Iwasaki, and K. Yamanouchi, *Nat. Commun.* **6**, 8347 (2015).

- [20] J. Yao, S. Jiang, W. Chu, B. Zeng, C. Wu, R. Lu, Z. Li, H. Xie, G. Li, C. Yu, Z. Wang, H. Jiang, Q. Gong, and Y. Cheng, Phys. Rev. Lett. **116**, 143007 (2016).
- [21] A. Azarm, P. Corkum, and P. Polynkin, Phys. Rev. A **96**, 051401(R) (2017).
- [22] L. Arissian, B. Kamer, Rastegari.A., D. Villeneuve, and J. Diels, Phys. Rev. A **98**, 053438 (2018).
- [23] M. Britton, P. Laferrière, D. Ko, Z. Li, F. Kong, G. Brown, A. Naumov, C. Zhang, L. Arissian, and P. Corkum, Phys. Rev. Lett. **120**, 133208 (2018).
- [24] M. Britton, M. Lytova, P. Laferrière, P. Peng, D. Ko, P. Polynkin, D. Villeneuve, C. Zhang, M. Spanner, L. Arissian, and P. Corkum, Phys. Rev. A **100**, 013406 (2019).
- [25] D. Kartashov, S. Haessler, S. Ališauskas, G. Andriukaitis, A. Pugžlys, A. Baltuška, J. Möhring, D. Starukhin, M. Motzkus, A. M. Zheltikov, M. Richter, F. Morales, O. Smirnova, M. Y. Ivanov, and M. Spanner, in *Research in Optical Sciences (Optical Society of America, Washington, 2014)*, p. HTh4B.5.
- [26] A. Mysyrowicz, R. Danylo, A. Houard, V. Tikhonchuk, X. Zhang, Z. Fan, Q. Liang, S. Zhuang, L. Yuan, and Y. Liu, APL Photonics **4**, 110807 (2019).
- [27] O. Kocharovskaya, Phys. Rep. **219**, 175 (1992).
- [28] O. Kocharovskaya and Y. Khanin, Pis'ma Zh. Eksp. Teor. Fiz. **48**, 581 (1988), [JETP Lett. **48**, 630 (1988)].
- [29] Y. Khanin and O. Kocharovskaya, J. Opt. Soc. Am. B **7**, 2016 (1990).
- [30] M. Richter, M. Lytova, F. Morales, S. Haessler, O. Smirnova, M. Spanner, and M. Ivanov, ArXiv:2001.08081 (submitted, 2020).
- [31] L. Klynning and P. Pagès, Phys. Scr. **25**, 543 (1982).
- [32] G. Herzberg, *Molecular Spectra and Molecular Structure: Volume I - Spectra of Diatomic Molecules.*, 2nd ed. (Krieger Publishing Company, Florida USA, 1989).
- [33] R. Boyd, *Nonlinear Optics*, 3rd ed. (Elsevier, Academic Press, 2008).
- [34] L. Keldysh, Zh. Eksp. Teor. Fiz. **47**, 1945 (1964), [Sol. Phys. JETP Lett. **20**, 1307 (1965)].
- [35] D. Pavičić, K. Lee, D. Rayner, P. Corkum, and D. Villeneuve, Phys. Rev. Lett. **98**, 243001(4) (2007).
- [36] M. Spanner and S. Patchkovskii, Chem. Phys. **414**, 10 (2013).
- [37] M. Schmidt, K. Baldrige, J. Boatz, S. Elbert, M. Gordon, J. Jensen, S. Koseki, N. Matsunaga, K. Nguyen, S. Su, T. Windus, M. Dupuis, and J. Montgomery Jr, J. Comput. Chem. **14**,

1347 (1993).

- [38] R. Bullough, P. Jack, P. Kitchenside, and R. Saunders, *Physica Scripta* **20**, 364 (1979).
- [39] A. Quarteroni, R. Sacco, and F. Saleri, *Numerical Mathematics*, 2nd ed. (Springer-Verlag Berlin Heidelberg, 2007).
- [40] J. Strikwerda, *Finite Difference Schemes and Partial Differential Equations.*, 2nd ed. (Society for Industrial and Applied Mathematics (SIAM), Philadelphia, PA, 2004) pp. xii+435.

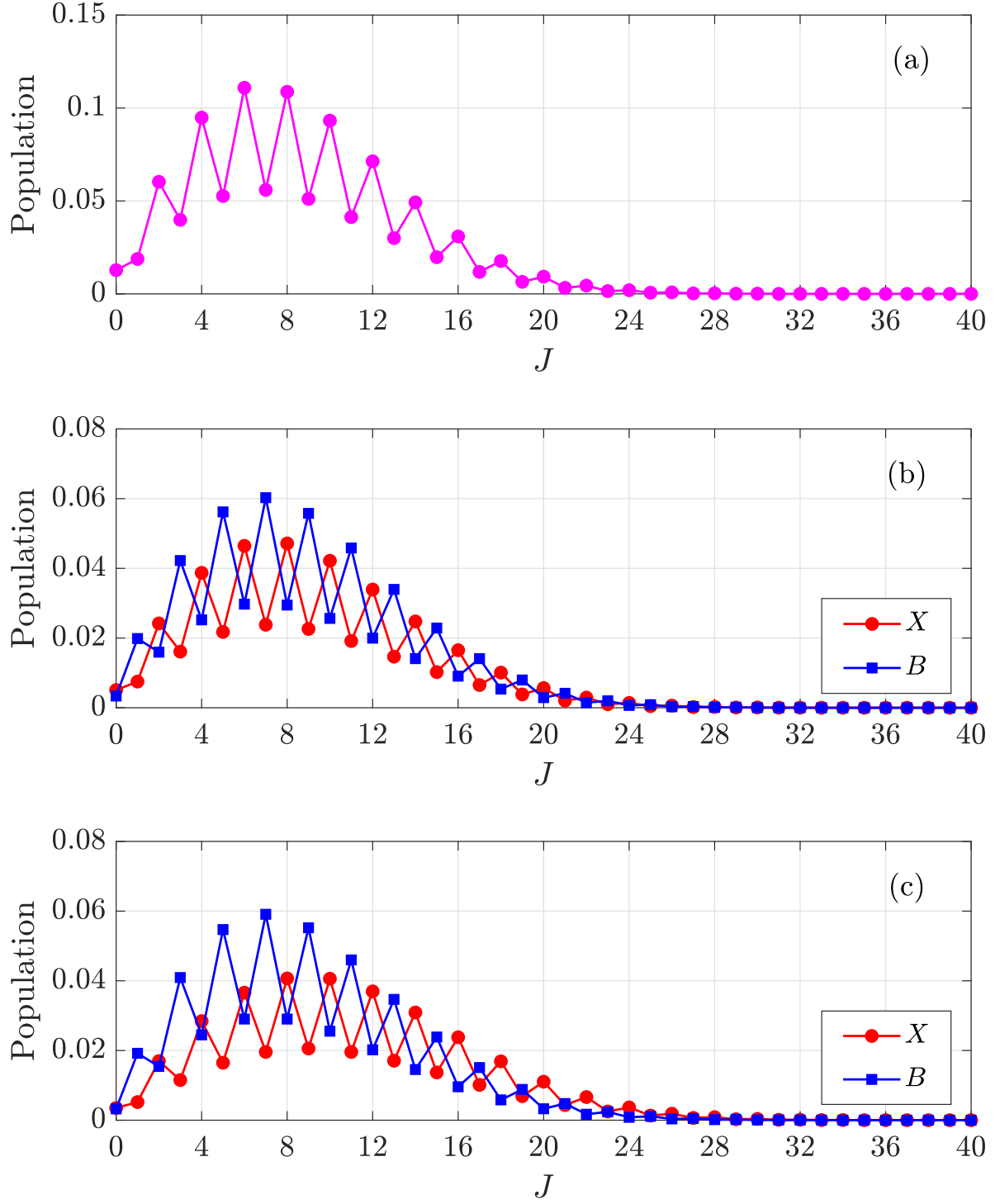


FIG. 2. (a) Initial thermal rotational distribution in the neutral with temperature $T = 298$ K. (b) Rotational populations on the X and B ionic states after excitation/ionization by the pump pulse with intensity $I_{pump} = 1 \times 10^{14}$ W/cm². The relative ionic populations are set to be $p_X = 0.45$ and $p_B = 0.55$. (c) Same parameters as (b) but with $I_{pump} = 2 \times 10^{14}$ W/cm².

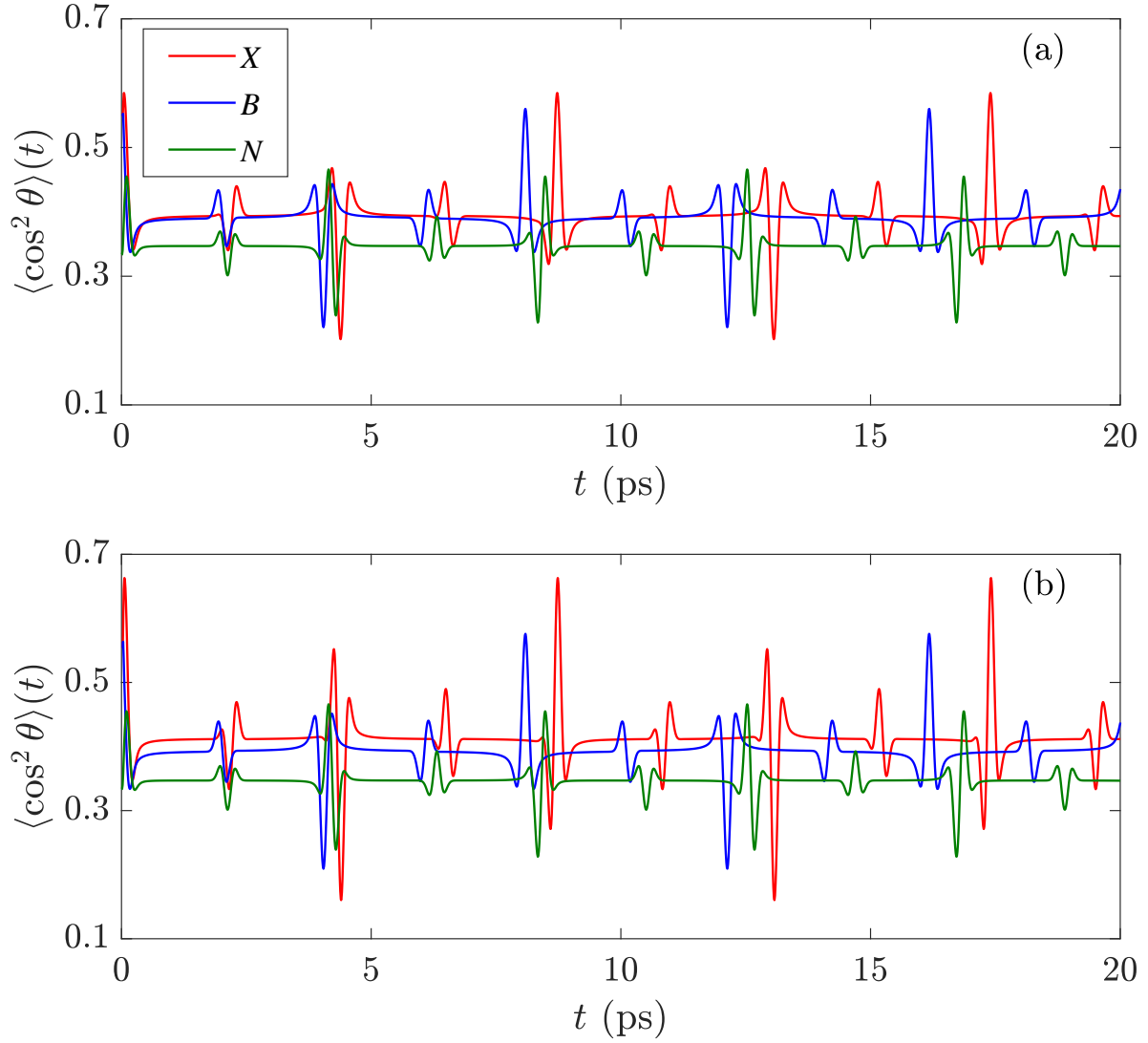


FIG. 3. Measures of the alignment $\langle \cos^2 \theta \rangle(t)$ for the neutral and ionic components at temperature $T = 298$ K. Panel (a) is for a pump intensity of $I_{pump} = 1 \times 10^{14}$ W/cm², while panel (b) is for $I_{pump} = 2 \times 10^{14}$ W/cm².

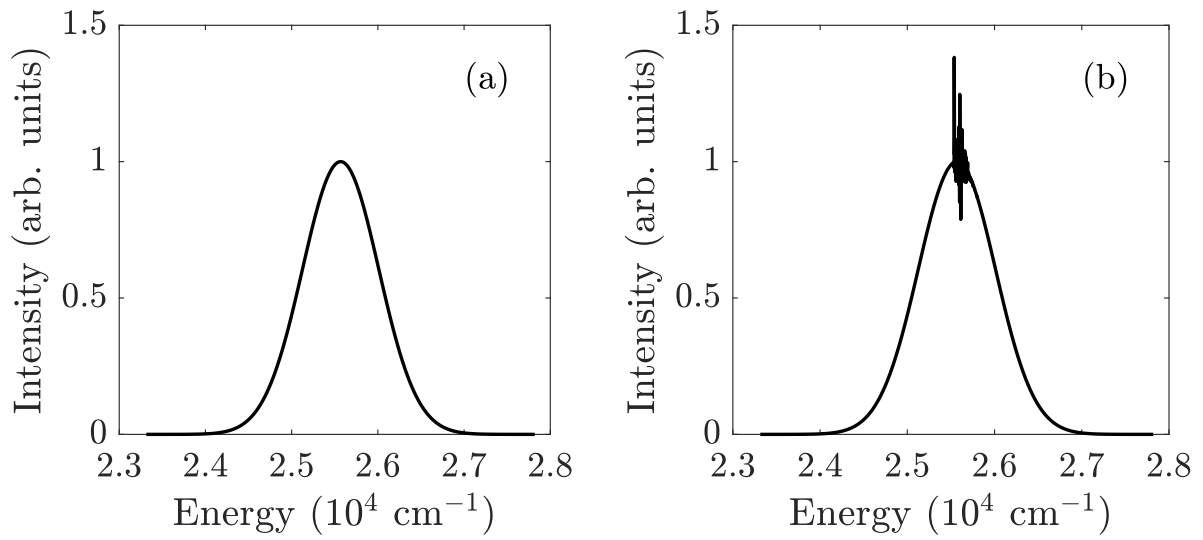


FIG. 4. (a) Input spectrum of the seed pulse, $\lambda_s = 391$ nm. (b) Output spectrum of the seed pulse for a delay of $t_{del} = 5$ ps and total propagation length of $z_{max} = 0.5$ mm. Gain/absorption lines can be seen near the peak of the output seed spectrum.

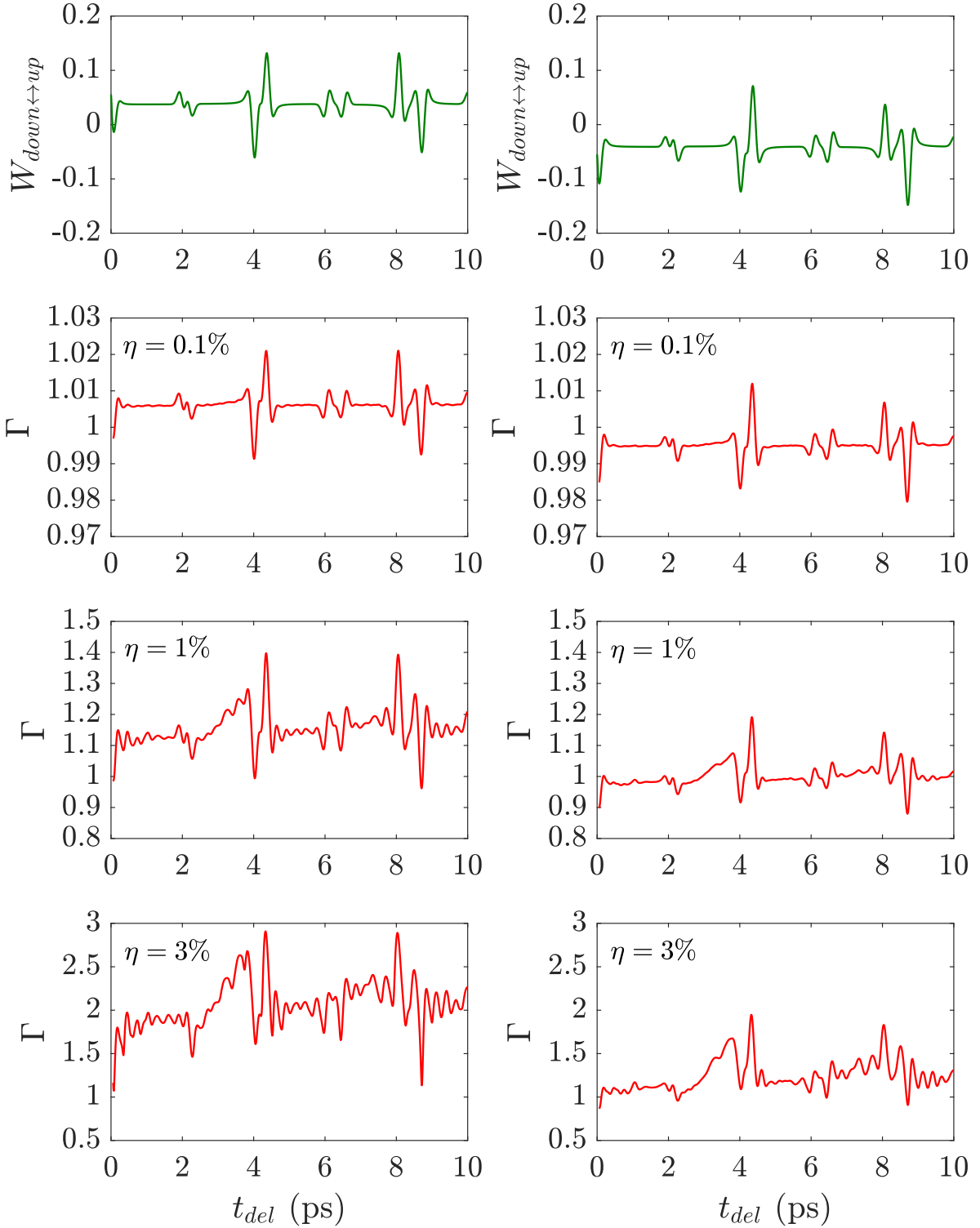


FIG. 5. Gain/absorption defined according to the perturbative estimate Eq. (49), and using the numerical spectrum to define the gain through Eq. (46). Left side corresponds to $p_X = 0.45$ and $p_B = 0.55$ (with electronic inversion), and the right side is for $p_X = 0.55$ and $p_B = 0.45$ (no electronic inversion). The results for Γ are presented for various ionization levels $\eta = 0.1\%$, 1% , and 3% as noted. Other simulation parameters are $z_{max} = 0.5$ mm, $\lambda_s = 391$ nm, $\sigma_s = 20$ fs, $I_{ump} = 10^{14}$ W/cm².

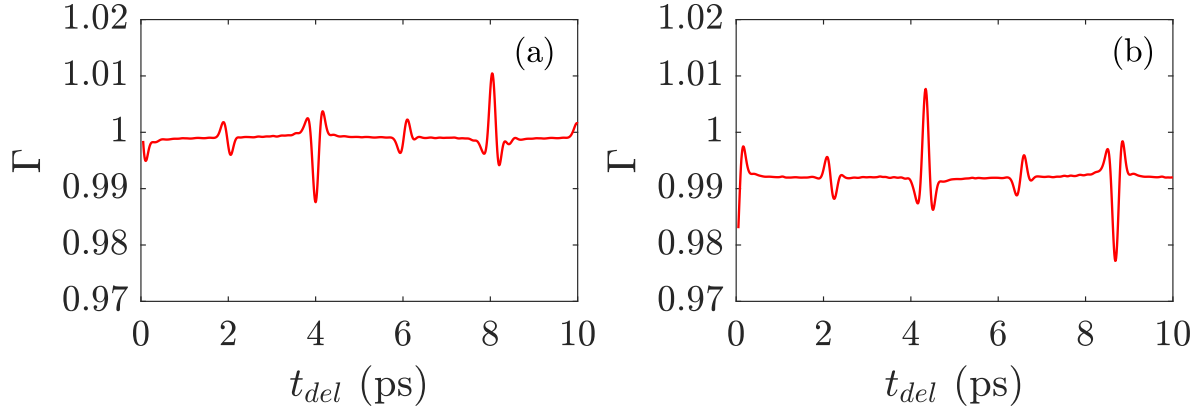


FIG. 6. Gain/absorption as a function of pump-seed delay t_{del} for hypothetical cases where (a) the X state was kept in a thermal distribution of rotational states, and (b) for the case where B was kept in a thermal distribution of rotational states. All other simulation parameters are the same as used in Fig.5 with $p_X = 0.55$ and $p_B = 0.45$ (no electronic inversion).

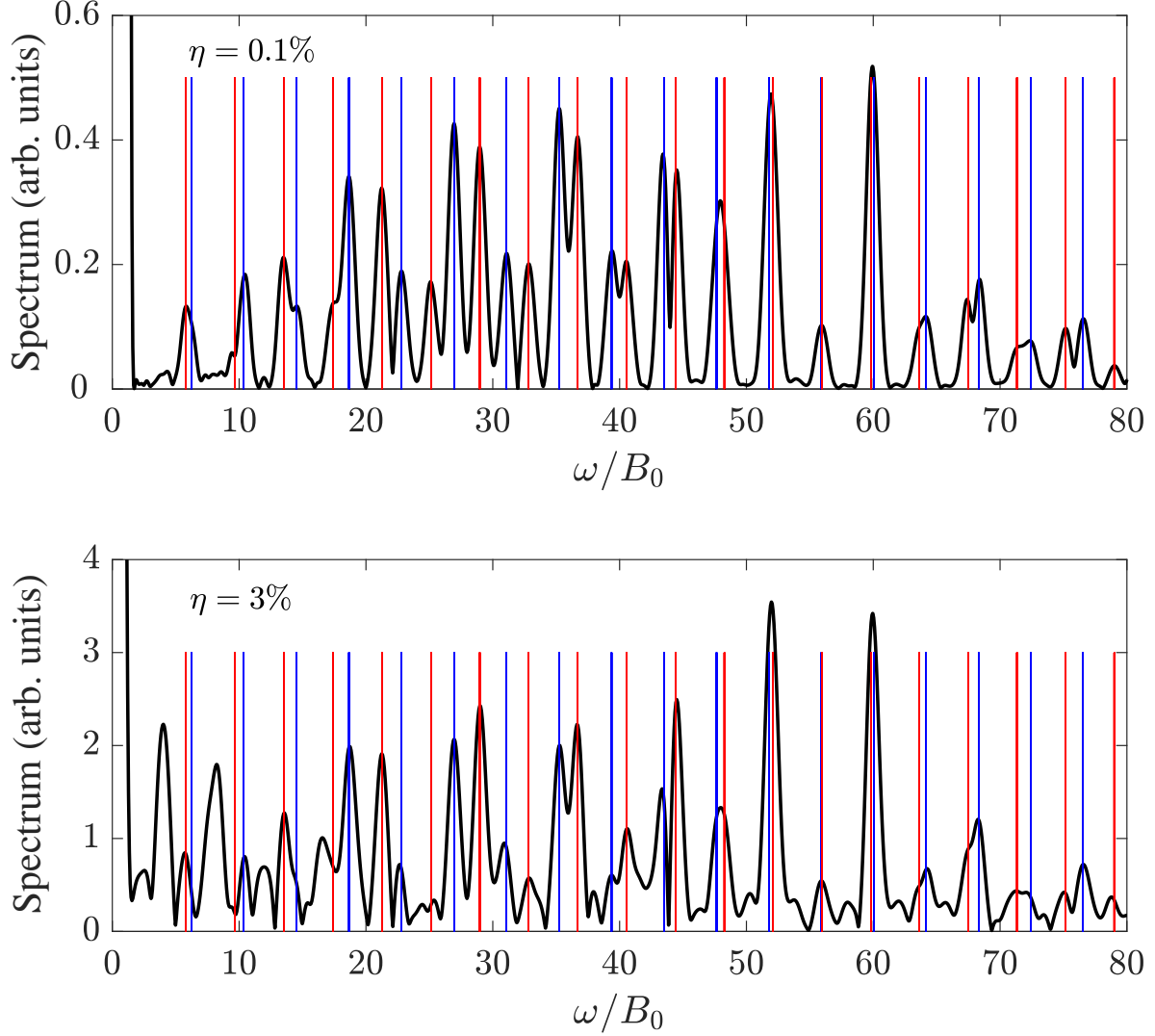


FIG. 7. Fourier transform of the delay-dependent gain/absorption signal $\Gamma(t_{del})$ for ionization fraction of $\eta = 0.1\%$ and 3% . The frequency axis has been normalized by the rotational constant of the neutral, which is labeled as B_0 on this plot. The red lines denote the expected positions of the X state peaks $\omega_J^X = \mathcal{E}_{J+2}^X - \mathcal{E}_J^X$, while the blue lines denote the expected positions for the B state $\omega_J^B = \mathcal{E}_{J+2}^B - \mathcal{E}_J^B$. These simulations are for the same parameters used in Fig.5, and correspond to the $p_X = 0.45$ and $p_B = 0.55$ case.

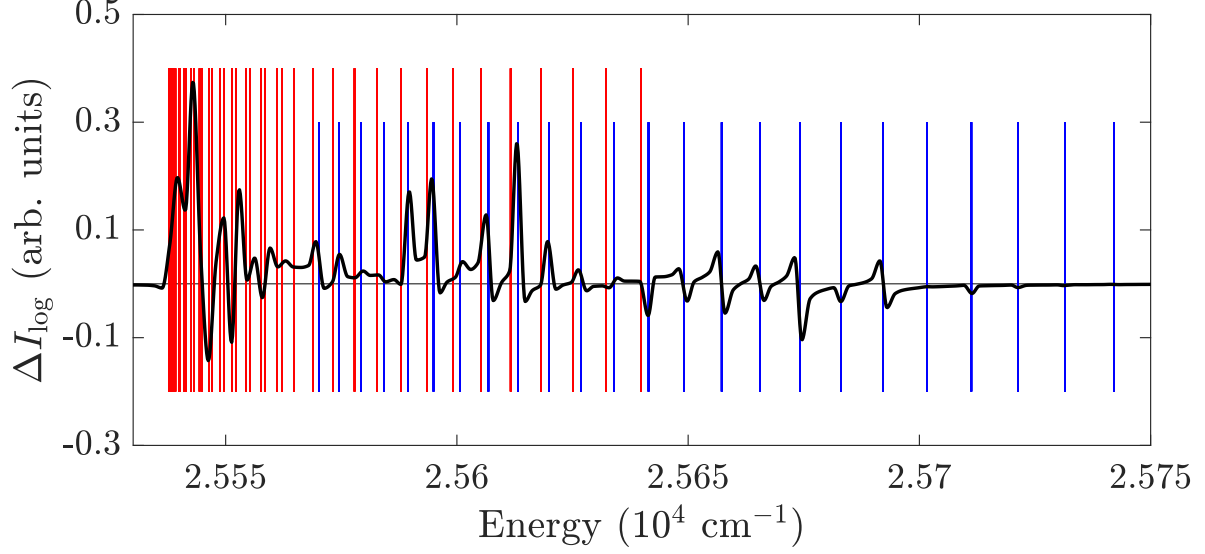


FIG. 8. Gain and absorption lines in the output spectrum of the seed pulse for a delay of $t_{del} = 4.3$ ps. All simulation parameters are the same as used in Fig.5 with $\eta = 0.1\%$, $p_X = 0.45$ and $p_B = 0.55$. Plotted is the difference between the output and input spectrum, ΔI_{\log} [see Eq. (59)], across the range of energies corresponding to the $B \leftrightarrow X$ transitions. The red lines denote the P-branch transitions, while the blue lines show the R-branch transitions (see Fig.1).

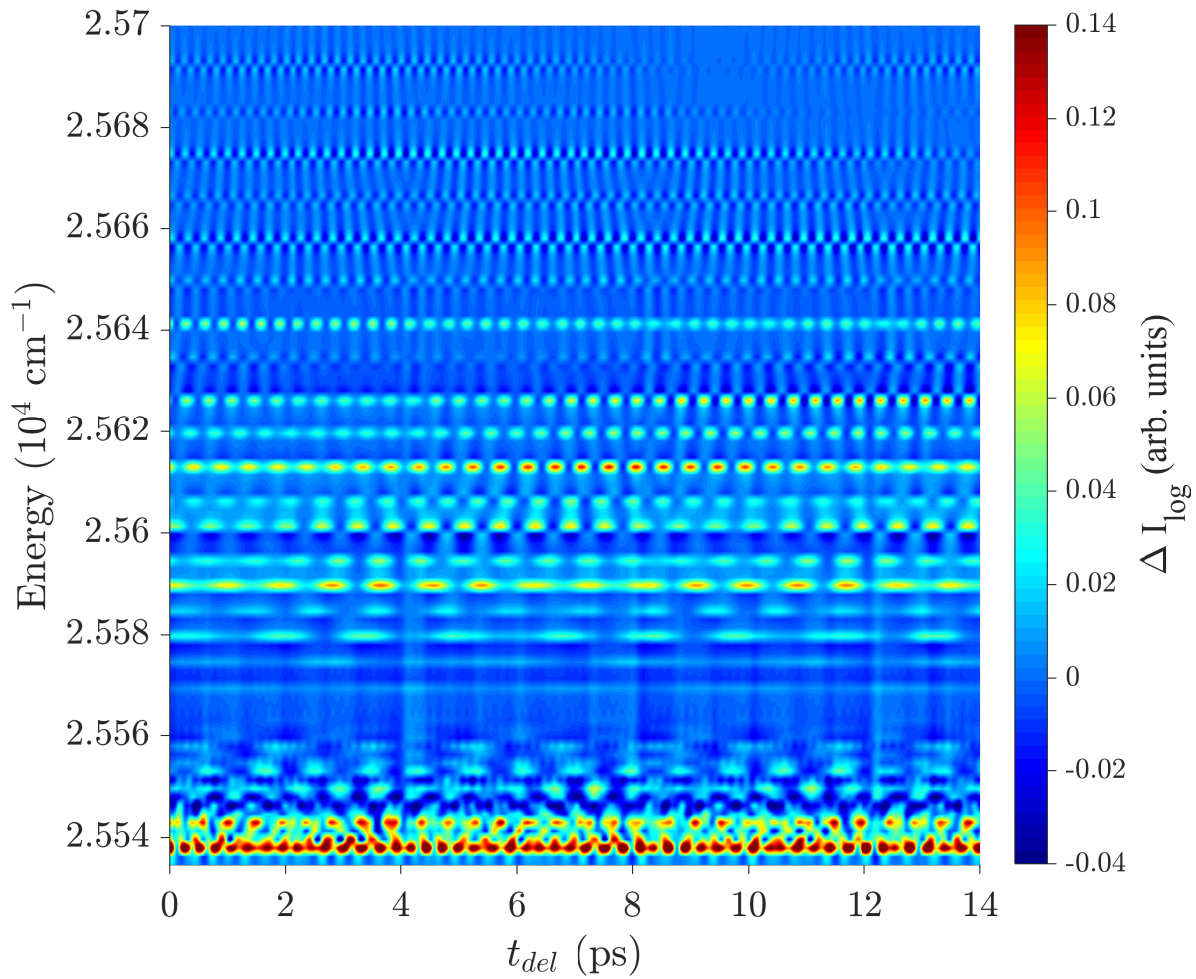


FIG. 9. Delay dependence of the gain and absorption lines in the output seed spectrum. As in Fig. 8, ΔI_{\log} [see Eq. (59)] is plotted across the $B \leftrightarrow X$ transition region.